EARTHQUAKE ENGINEERING AND STRUCTURAL DYNAMICS, VOL. 25, 1275–1299 (1996)

THE SEISMIC RESPONSE OF CONCENTRICALLY BRACED MOMENT-RESISTING STEEL FRAMES

LUCA MARTINELLI, MARIA GABRIELLA MULAS AND FEDERICO PEROTTI
Department of Structural Engineering, Politecnico di Milano, Piazza Leonardo da Vinci 32, 20133 Milano, Italy

SUMMARY

The paper deals with the dynamic non-linear behaviour of concentrically braced steel moment-resisting frames under severe earthquake conditions. The first part of the paper is devoted to the description of a non-linear beam element which has been developed starting from the classical 'one-component' formulation, having concentrated inelastic hinges at the ends. The hysteretic behaviour of the end hinges is calibrated on the basis of a set of experimental tests previously performed at Politecnico di Milano. The non-linear brace element used to model the diagonal bars and the procedure for step-by-step dynamic analysis are then briefly summarized.

In the second part of the paper two examples of application are presented; the first one concerns a six-storey MRF designed in accordance with Eurocode 8, in which concentric braces are introduced only to satisfy the serviceability limit state requirements (interstory drifts) but are not taken into account in the ultimate conditions. The numerically computed seismic behaviour of the system is analysed and compared to that of the unbraced frame. The second example is a six-storey CBF designed according to the Eurocode 8 specifications; the non-linear behaviour under seismic loading is studied especially to the aim of analysing the effect of the columns flexural stiffness and resistance, which was not considered in the design, on the CBF response.

KEY WORDS: moment-resisting steel frames; concentrical bracing; dynamic non-linear behaviour

1. INTRODUCTION

Moment-resisting frames (MRFs) and concentrically braced frames (CBFs) are by far the most common steel structural systems used to absorb seismic forces. None of the two systems is deemed to possess a completely satisfactory behaviour under seismic actions.

MRFs, when properly designed, detailed and constructed, can show very good dissipation properties under extreme seismic conditions, but can perform poorly, due to excessive lateral deformability, against moderate earthquakes, allowing for intolerable non-structural damage. For this reason modern codes, such as Eurocode 8 (EC8 in the following),[1] prescribe very strict deformation (interstory drift) limits which, in many cases, actually control structural design, leading to the choice of structural elements which are largely oversized in terms of resistance.

In addition, experience from the recent Northridge earthquake[3] shows that, even though no partial nor total collapse of steel MRFs occurred, a large number of beam-to-column welded connection failures was detected after inspection of buildings. A subsequent case study, regarding one of the damaged buildings, resulted in numerically estimated plastic rotation demands of about 0·02, which justify, on the basis of experimental evidence, the observed joint cracking.

CBFs, on the other hand, show very good lateral stiffness properties but, as it concerns energy dissipation under strong seismic actions, almost completely rely on the hysteretic behaviour of the diagonal bars, which are subjected alternatively to buckling in compression and yielding in tension. Such behaviour can show significant degradation both in stiffness and in loading capacity,[4,5] so that the overall dissipation capability can undergo dramatic decay during the earthquake loading process; moreover, multistory frames often show 'soft-storey' problems[6] which can increase local ductility demands significantly. For the quoted reasons, code provisions[1,2] tend to prescribe for CBFs' design very strict rules, which can be summarized as follows:

CCC 0098–8847/96/111275–25

Received 1 March 1996
Revised 14 June 1996

(a) design forces higher than the ones for MRFs (lower behaviour coefficients);
(b) low slenderness ratios for diagonal members;
(c) neglect the resistance of the compressed diagonal (in EC8), regardless of the bar slenderness;
(d) strict overstrength conditions for the design of the diagonal end connections, which become even more severe when combined with rules (a) and (b) which lead to quite heavy bracing members.

Nevertheless, it must be noted that, in many countries and especially for industrial facilities, CBFs still represent the preferred design solution for lateral loads.

Summing up, further investigation about the behaviour of MRF and CBF structural systems under strong seismic actions appears still to be worthwhile. In fact, an effort towards a better characterization of the plastic deformation demands in both systems is largely justified by the above considerations; in addition, given the dual characteristics of MRFs and CBFs in terms of stiffness and energy dissipation capabilities, it seems valuable to investigate how the possible interaction between the two systems can be effectively exploited.

In this light considerable research effort has been devoted to beam modelling, by developing a lumped plasticity element whose inelastic hinges behaviour (moment–rotation relation) is based upon experimental tests. The problems arising from the implementation of the model within a step-by -step implicit integration procedure have also been solved by adopting, at the element level, an event-to-event strategy.

Finally, the research work here presented focuses attention on two examples of structural systems in which the MRF and CBF resisting mechanisms are only partially combined, i.e. without leading to the design of a traditional dual system. More precisely, the dynamic behaviour of the following combined systems has been investigated.

System CS1: It is a MRF frame which is traditionally designed, following EC8,[1] against ultimate seismic actions, without checking serviceability limit state provisions against moderate seismic events. To fulfill the latter requirements concentrical braces are inserted in the frame, which do not satisfy EC8 rules for diagonal members, since they are not considered in the collapse resistance of the structural system. The dynamic analysis of the combined system has been performed to compare its behaviour to that of the unbraced frame, in terms of overall response and local ductility demands.

System CS2: It is a traditional CBF system, which differs from standard design practice only in that the column section orientation (which are made of HEB wide-flange sections) is such that maximum flexural stiffness and resistance lies in the CBF plane. For this reason, given the column continuity, which is usually achieved in practice even though neglected in the design, and considering the relatively large column size which is necessary to satisfy capacity design provisions, vertical members have been modelled as non-linear frame elements in the numerical simulation of the CBF seismic response. Note that the contribution of columns flexural stiffness and resistance is not intended to be considered in the structural design, but was here considered just to analyse its possible effect in improving the CBF overall behaviour.

The dynamic non-linear behaviour of the above described systems has been investigated by means of a step-by-step numerical procedure, whose main features will be summarized in Section 4 of the paper. In Section 3, a brief description of the non-linear truss element used for brace modelling, which has been described in detail in References 4 and 5, is given, while Section 2 is devoted to a thorough presentation of the non-linear beam element. In Sections 5 and 6, the assumptions made in the design and the results obtained in the analysis of the quoted systems will be described.

2. THE BEAM ELEMENT

The critical areas of plane MRFs loaded by strong earthquakes are usually located close to the beam–column joint interfaces. Inelastic phenomena start in these cross-sections; in the case of steel structures the experimental evidence[7] shows that phenomena such as low-cycle fatigue and local buckling prevent the spreading of plasticization. For this reason the beam element developed in the present work is based upon a lumped-plasticity model, known in the literature as 'one-component' model.[8] In such a model it is supposed that the non-linear effects, due to bending alone, do not spread along the length of the beam, being ideally concentrated over a part of zero length, the plastic hinge, forming at each end of the beam.

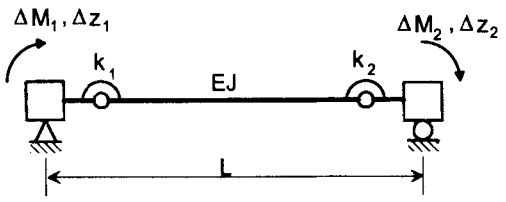

Figure 1. Non-linear beam element

The beam model, depicted in Figure 1, is composed of a central part, of length L equal to the length of the element to be modelled, linked in series (at each end) with a hinge having a rotational spring, called a plastic hinge in the following. The central part has elastic behaviour; inelastic phenomena take place only in the plastic hinges, having rigid-plastic behaviour, since in the linear range the element flexibility is entirely due to the central beam. Plastic hinges can follow different, independent, hysteretic relationships. The element flexibility matrix, referred to the degrees of freedom of Figure 1, namely the rotation of the two ends relative to the chord, is easily found by summing up contributions of beam and plastic hinges:

$$[f] = [f_b] + [f_s] = \begin{bmatrix} f_{b_{11}} & f_{b_{12}} \\ f_{b_{21}} & f_{b_{22}} \end{bmatrix} + \begin{bmatrix} f_{s_1} & 0 \\ 0 & f_{s_2} \end{bmatrix} \tag{1}$$

The local stiffness tangent matrix $[k]$ is then determined by inversion of the flexibility matrix $[f]$ and the stiffness matrix $[K]$ of the element, taking into account also rigid body modes (i.e. vertical translations), is obtained by transforming $[k]$ according to a suitable transfer matrix $[T]$:

$$[K] = [T]^{\mathrm{T}}[k][T] \tag{2}$$

The matrix $[T]$ can easily take into account the occurrence of rigid ends outside the element, modelling a rigid beam-to-column joint. Axial stiffness, not being considered here, is uncoupled from flexural stiffness, and has the standard expression for elastic bars. Shearing deformation can be easily accounted for by giving the appropriate value to the coefficients in the expression of $[f_b]$.

Two problems arise with the adoption of this model, one related to the state determination of the element (computation of internal restoring forces), and the other with the determination of the hysteretic relation for plastic hinges. The former was already pointed out by Giberson,[8] who remarked that backtracking and overshooting phenomena are unavoidable if the simple formulation in terms of flexibility is used to determine internal forces in the element; the latter arises from the need of attributing to plastic hinges a moment–rotation hysteretic relationship capable of reproducing the experimental evidence. The solution of these two problems is addressed in the following sections.

2.1. The hysteretic relation for plastic hinges

Inelastic phenomena occurring at the ends of a beam are never lumped rigorously in a single cross-section; however, the concept of plastic hinge can be adopted successfully when the spreading of inelasticity is limited to a portion of the beam having approximately the same length of the characteristic dimension of the cross-section, as it happens in steel I-beams commonly adopted for frame structures. The hysteretic moment–rotation law for plastic hinges must be able to represent the inelastic phenomena taking place over a very short length of the beam: however, it cannot be thought off simply as derived by integration of a moment–curvature relationship, since this is unable to take into account phenomena that involve a finite length of the beam, such as local buckling. Therefore, the sought moment–rotation relation for the plastic hinge has been directly derived from a constitutive model[9] given in terms of global parameters, namely force and displacement at the free end of a cantilever beam. In the following the force–displacement relation will be briefly summarized, and the analytical procedure to derive the moment–rotation relation will be thoroughly presented.

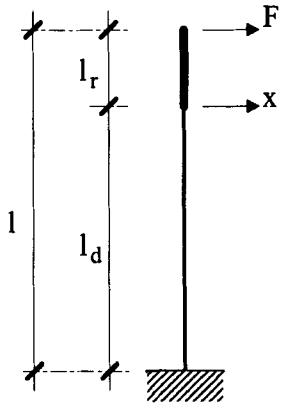

Figure 2. Scheme of experimental test on cantilever member

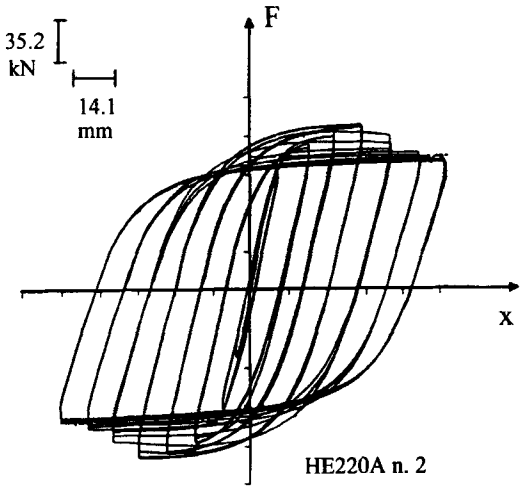

Figure 3. Example of experimental test result: load vs. displacement cyclic response

2.1.1. The force–displacement relation. The constitutive model (see Reference 10) describes the experimental non-linear behaviour of a cantilever beam subjected to cyclic loading. The experimental setting is schematically shown in Figure 2; for reasons inherent to the geometry of the testing machine, the cantilever beam, having length l, is composed of a deformable part of length l_d and of a rigid part of length l_r. A force F is applied on the specimen top, while the displacement x is read at the top of the deformable part. A typical F–x experimental diagram is depicted in Figure 3 for an HE200A beam; the main features of the experimental F–x relation are the following.

(1) The primary curve shows an elastic–plastic behaviour, allowing for a reasonable determination of the force and displacement at first yielding, namely, F_y and x_y.
(2) The generic hysteresis cycle is composed of three branches characterized by different behaviours; a stiffness degraded reloading branch, a yielding branch and an elastic unloading branch. The damage accumulated in the specimen, due to buckling of compression flanges, fatigue and fracture, causes a decrease in the stiffness of reloading and yielding branches, and reduces the specimen strength, by modifying the force level at which the start of yielding occurs; the latter effect is counteracted by isotropic strain-hardening, which leads, on the contrary, to an expansion of the area subtended by the cycle.

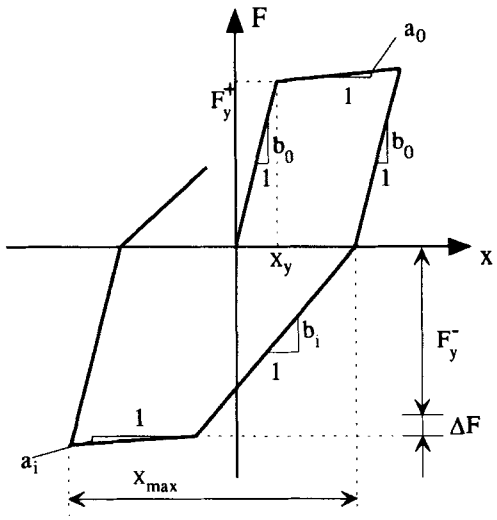

Figure 4. Analytical force vs. displacement hysteretic curve

A trilinear constitutive model was adopted in Reference 9 to represent the described behaviour. The primary curve, symmetric, is bilinear, and is completely defined by the elastic stiffness b_0, the initial yielding stiffness a_0, and by the yielding point (F_y, x_y). The generic hysteresis cycle is represented by a trilinear curve (Figure 4); the stiffness degraded reloading branch and the yielding branch at the ith cycle have stiffness b_i and a_i, respectively, these values being lower than the initial values b_0 and a_0; unloading takes always place with the elastic stiffness b_0; reloading following a partial unloading is elastic up to the unloading point. The amount of stiffness reduction is related to the semi-cycle maximum amplitude x_{max} (see Figure 4) previously experienced, the latter being defined as the difference, in absolute value, between the value of x for $F = 0$ and the value reached at the following reversal point. The parameter x_{max} is defined (and consequently updated) only for 'complete' cycles, where the reversal point lies on the yielding branch (Figure 4). By denoting $\bar{F} = F/F_y$, $\bar{x} = x/x_y$, and with $\bar{a}$ and $\bar{b}$ the stiffnesses a and b in the $\bar{F}$–$\bar{x}$ plane, the following relations hold:[9]

$$\bar{a}_i = \bar{a}_0(1 - H_1 \bar{x}_{max}) \tag{3}$$

$$\bar{b}_i = \bar{b}_0(1 - H_2 \bar{x}_{max}) \tag{4}$$

The non-dimensional, positive, coefficients H_1 and H_2 have been set[9] from the experimental curves. The onset of yielding in the generic ith cycle will occur, on positive and negative side, respectively, at a value F_y^+ or F_y^- given by:

$$F_y^+ = F_y + \Delta F_y \tag{5}$$

$$F_y^- = -F_y - \Delta F_y \tag{6}$$

In equations (5) and (6) ΔF_y is the translation undergone by the yielding branch with respect to the initial value F_y; this translation is expressed in non-dimensional form as:

$$\Delta \bar{F}_y = H_3 \bar{x}_{max} - H_4 \bar{x}_b - \sum_{j=1}^{i-1} H_5 \bar{x}_j \tag{7}$$

In equation (7) H_3, H_4 and H_5 are non-dimensional, positive coefficients, set on the basis of experimental data; the first term accounts for isotropic strain hardening, the second one for the loss of strength due to buckling of compression flanges and the third one for damage due to low-cycle fatigue. The non-dimensional

displacement $\bar{x}_b$ is the buckling effective displacement, defined as

$$\bar{x}_b = \bar{x}_{\max} - \bar{x}_{fb} \geqslant 0 \tag{8}$$

$\bar{x}_{fb}$ being the absolute value of the non-dimensional semi-cycle amplitude preceding the first occurrence of local buckling. The parameter $\bar{x}_{\max}$ appearing in the previous equations cannot exceed an upper limit $\bar{x}_{\lim}$ depending on the cross-section geometry and set on the basis of experimental data.

2.1.2. The moment–rotation relation. The sought relation is derived through a change of reference global parameters in the force–displacement constitutive model; this change allows, on one hand, to determine the moment–rotation relation needed for plastic hinges and, on the other hand, to make the constitutive model independent of the particular geometry of the specimen used for the experimental tests.

The main purpose of this change is to describe the M–β relation of a hypothetic plastic hinge lying at the bottom of the cantilever beam and accounting for the inelastic phenomena taking place in the beam itself. The new parameters are therefore the moment M at the bottom of the beam and the rotation β undergone by the chord of the deformable part of the beam, due to the inelastic part x_p of the displacement x; with reference to Figure 2 we obtain:

$$M = Fl \tag{9}$$

$$\beta = \frac{x_p}{l_d} \tag{10}$$

In a non-dimensional form the above parameters become:

$$\bar{M} = \frac{M}{M_y} \tag{11}$$

$$\bar{\beta} = \frac{\beta}{\beta_y} = \frac{x_p}{x_y} = \bar{x}_p \tag{12}$$

The values M_y and β_y are obtained from equations (9) and (10), resepectively, when $F = F_y$ and $x_p = x_y$. The rotation β_y is only a reference value and does not have the physical meaning of rotation in the plastic hinge when $M = M_y$, since β is identically zero in the elastic range up to F_y. Equations (9)–(12) hold also in an incremental sense; in particular, it results in

$$\Delta\bar{\beta} = \Delta\bar{x}_p \tag{13}$$

and, from equations (9) and (11) the following equality descends:

$$\Delta\bar{M} = \Delta\bar{F} \tag{14}$$

It is now necessary to determine how the change of parameters modifies both the non-dimensional tangent stiffness $\bar{k}$ in the $\bar{F}$–$\bar{x}$ plane and the semi-cycle maximum amplitude $x_{\max}$, together with the related values x_b, x_{fb} and $x_{\lim}$. For this purpose, it is easy to see that, in the elastic range, we can write, both in finite and incremental terms:

$$\bar{F} = \frac{F}{F_y} = \frac{k_e x_e}{k_e x_y} = \bar{x}_e; \qquad \Delta\bar{F} = \Delta\bar{x}_e \tag{15}$$

Moreover, the following equation holds by simply giving to $\bar{k}$ the value which is appropriate for the considered range (elastic, strain-hardening, unloading, reloading):

$$\Delta\bar{F} = \bar{k}\,\Delta\bar{x} \tag{16}$$

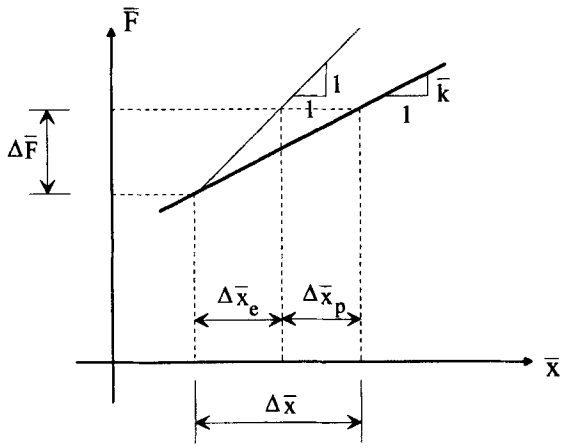

Figure 5. Elastic and inelastic contributions to the displacement increment

The increment $\Delta\bar{x}$ can be thought off as the sum of an elastic and an inelastic component (see Figure 5):

$$\Delta\bar{x} = \Delta\bar{x}_e + \Delta\bar{x}_p \tag{17}$$

Taking into account equations (15) and (16), the inelastic component of the displacement increment can be written as:

$$\Delta\bar{x}_p = \Delta\bar{x} - \Delta\bar{x}_e = (1 - \bar{k})\Delta\bar{x} \tag{18}$$

Finally, by taking into account equations (14), (16) and (18) the relation between $\Delta\bar{M}$ and $\Delta\bar{\beta}$ is derived:

$$\Delta\bar{M} = \Delta\bar{F} = \bar{k}\,\Delta\bar{x} = \frac{\bar{k}}{1-\bar{k}}\Delta\bar{x}_p = \frac{\bar{k}}{1-\bar{k}}\Delta\bar{\beta} \tag{19}$$

From this equation it is apparent that in the elastic range [$\bar{k} = 1$, equation (15)] the plastic hinge has an infinite stiffness, i.e. a rigid behaviour.

Finally, it is necessary to determine how the cycle amplitude x_{max} transforms due to the change of parameters. For this purpose, giving to $\bar{x}$ the meaning of cycle amplitude, we can write equation (17) in a finite form:

$$\bar{x} = \bar{x}_e + \bar{x}_p \tag{20}$$

The elastic part $\bar{x}_e$ of the cycle amplitude $\bar{x}$ is directly related to the current value $F(t)$ of the force, and therefore of the moment $M(t)$, through equations (15) and (16); the inelastic part $\bar{x}_p$ is computed from the difference between the current value $\beta(t)$ of the plastic hinge rotation and the rotation β_0 at the last point where $M = 0$, i.e.:

$$\bar{x}_p = \frac{\beta(t) - \beta_0}{\beta_y} \tag{21}$$

The sought value of the cycle amplitude in terms of moment M and rotation β is then found, consistently with the definition given in Section 2.1.1:

$$\bar{x} = \frac{|M(t)|}{M_y} + \frac{|\beta(t) - \beta_0|}{\beta_y} \tag{22}$$

Equation (22) allows for the use of equations (3), (4), (7), (8), thus completing the transformations needed for the change of parameters in the constitutive model.

2.2. The state determination for the beam element

The process of an element state determination, in the framework of the direct stiffness method usually adopted by structural codes, requires the determination of the element nodal forces, given the nodal displacements computed by solving a set of simultaneous equations expressing the structure equilibrium conditions. This process is usually accomplished in three steps:

(a) The internal generalized deformations of the element are determined through geometric–kinematic considerations from nodal displacements, so that compatibility requirements are satisfied at a local level.
(b) The internal generalized actions of the element are computed from generalized deformations, making use of a generalized action–deformation relation.
(c) Nodal forces are computed from internal actions by simple statics, imposing the element equilibrium.

The state determination of the adopted model cannot be carried out according to this procedure. In fact, as this is a model defined in terms of flexibility, step (a) is not defined and the end rotations $\{\Delta z\}$ are subdivided into the contributions $\{\Delta w\}$ and $\{\Delta\beta\}$, provided, respectively, by the central beam and the springs, on the basis of the simple formulation seen above; this implies that step (b) is performed in the reverse way, i.e. computing generalized deformations from generalized actions. Problems arise when, during a generic load step, the tangent stiffness in the hysteretic moment–rotation relationship of any one of the plastic hinges changes. In this case, if the subdivision of $\{\Delta z\}$ into $\{\Delta w\}$ and $\{\Delta\beta\}$ is unaffected by this change, the correct state determination of the spring itself will cause necessarily an unbalanced moment at the beam–spring interface, since the central beam has an elastic behaviour. These unbalanced moments cannot be eliminated and will accumulate, thus causing an error, of unknown importance, in the determination of structural response.

The problem can be correctly focused by pointing out that the insertion of a spring inside a beam element adds to the element itself a further degree of freedom. This degree of freedom is implicitly condensed out when the stiffness matrix of the element is derived by inversion of the flexibility matrix, but should be taken explicitly into account when unbalanced moments are acting on it. However, as springs exhibit a rigid–plastic behaviour, the standard static condensation procedure cannot be used when the spring tangent stiffness is infinite.

An alternative solution to this problem has been found in the adoption, at the element level, of an event-to-event strategy, having defined as an event, in the generic plastic hinge, a change in the tangent stiffness of the moment–rotation relation. The strategy is developed according to the procedure summarized in the following.

(1) At the end of the generic load step the end rotation increments $\{\Delta z\}$ are known; the corresponding end moment increments, $\{\Delta M'\}$, can be computed, under the hypothesis that the tangent stiffness does not change during the step, according to the relation:

$$\{\Delta M'\} = [k]\{\Delta z\} \tag{23}$$

where $[k]$ is the element tangent stiffness at the beginning of the step. As central beam and springs are linked in series, the springs rotation increment is given by:

$$\{\Delta\beta'\} = [f_s]\{\Delta M'\} \tag{24}$$

(2) The springs state determination is performed, given $\{\Delta\beta'\}$, on the basis of the hysteretic relation M–β and of the values, at the beginning of the step, of the springs rotations and of the springs flexibility. If an event has occurred during the step, $[f_s]$ is changed and from the $M-\beta$ relation it is possible to compute both the springs flexibility $[f_{su}]$ at the end of the step and a factor μ such that $\mu\{\Delta M'\}$ are the moment increments producing the event. The constant μ (with $0 \leqslant \mu < 1$) is called event factor.

(3) Since the $M-\beta$ law is piecewise linear, the $\{M\}$–$\{z\}$ relation is linear too; as a consequence the vector $\{\Delta z\}$ can be scaled by the same event factor as $\{\Delta M\}$, and the increment of both moment and the springs rotation pertaining to the first part of the step can be computed as follows:

$$\{\Delta M_1\} = [k]\mu\{\Delta z\} \tag{25}$$

$$\{\Delta\beta_1] = [f_s]\{\Delta M_1\} \tag{26}$$

(4) The updated stiffness matrix $[k_u]$ can now be determined, by inserting $[f_{su}]$ in equation (1), and the remaining part of the step can be correctly performed as:

$$\{\Delta M_2\} = [k_u](1-\mu)\{\Delta z\} \tag{27}$$

$$\{\Delta\beta_2] = [f_{su}]\{\Delta M_2\} \tag{28}$$

(5) At the end of the step, the total increment of both the moment and springs rotation is given by:

$$\{\Delta M''\} = \{\Delta M_1\} + \{\Delta M_2\} \neq \{\Delta M'\} \tag{29}$$

$$\{\Delta\beta''] = \{\Delta\beta_1\} + \{\Delta\beta_2\} \neq \{\Delta\beta'\} \tag{30}$$

The advantage offered by this procedure lies in the fact that the element is internally in equilibrium, i.e. no unbalanced moments arise at springs–beam interface. The unbalanced moments (and consequently, shear forces produced by them) act only in points where nodal displacements are defined, along global coordinates, and can easily be eliminated by a standard Newton–Raphson procedure, or by any other strategy aiming to establish structural equilibrium in non-linear problems.

Finally, it can be useful to point out that the standard Newton–Raphson procedure also could have been applied, at the element level, to solve the problem of the state determination of this (and of any other) model defined in terms of flexibility. However, it was believed that this procedure, which does not require any iteration at the element level, can be more precise, effective and more easily implemented, especially in the case of piecewise linear hysteretic relationships.

3. THE NON-LINEAR TRUSS ELEMENT

The model adopted here for the behaviour of bars subjected to cyclic axial force (see References 4 and 6) is based on the discretization of the truss member into two rigid elements connected by a deformable cell [Figure 6(a)]; the model configuration is described by the cell's relative rotation ϕ and by the relative end displacement due to axial elongation, named u_n. The elastic properties of the cell (flexural and axial stiffness) are set in order to match the Euler critical load and the axial stiffness of the continuous bar.

The behaviour of the cell in the non-linear range is characterized on the basis of the properties of the cross-section of the bar; this is descretized into a finite number of strips [see Figure 6(b)] which are characterized by area, distance from section centroid, residual stress and yield limit. For each configuration change $(\Delta\phi, \Delta u_n)$, the deformation increments in the section strips are computed according to the following hypotheses:

(1) axial deformations are uniformly spread along the bar axis;
(2) plane sections remain plane;
(3) the ratio of the curvature to the elastic limit curvature in the midspan section of the bar equals the ratio of the rotation to the elastic limit rotation of the model cell.

Given the strain increment in each strip and the constitutive relation (here taken as elastic–plastic with kinematic hardening) the changes in the internal bending moment and axial forces

$$\Delta M = \Delta M(\Delta\phi, \Delta u_n); \qquad \Delta N = \Delta N(\Delta\phi, \Delta u_n) \tag{31}$$

can be computed by a simple summation process over the strips.

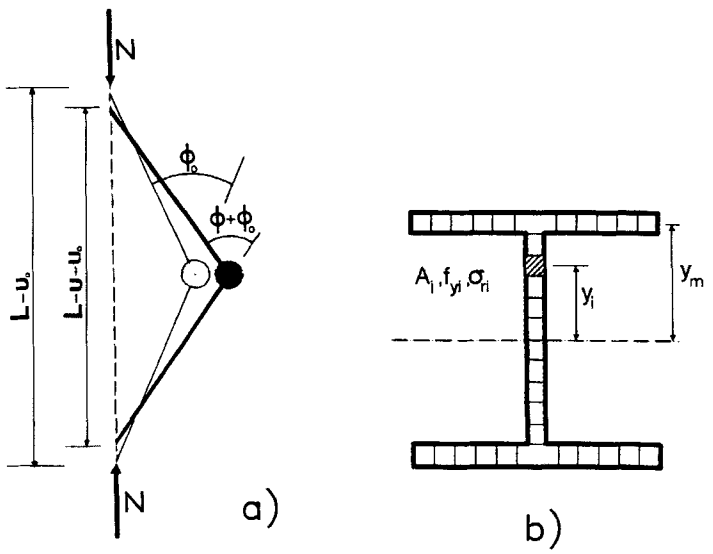

Figure 6. Non-linear truss element

Based upon the above criteria, the model allows for the incremental description of the relationship between the (total) relative end displacement Δu and the axial force ΔN; the relationship can be obtained, at each step, according to the following iterative procedure.

(a) Given the value of Δu two trial values of $\Delta\phi$ are chosen.
(b) The value of Δu_n is computed, for each value of $\Delta\phi$, satisfying the incremental second-order compatibility equation

$$\Delta u = \frac{L}{8}\Delta^2\phi + \frac{L}{4}(\phi + \phi_0)\Delta\phi + \Delta u_n \tag{32}$$

where ϕ is the current rotation and ϕ_0 is the value leading to the initial value of bar midspan out-of-straightness v_0.
(c) For each pair of values $(\Delta\phi, \Delta u_n)$, the changes in internal cell bending moment and axial force (31) are computed as summarized before.
(d) The equilibrium error Δe is computed, for each pair $(\Delta M, \Delta N)$, from the incremental equation

$$\Delta e = \Delta M - \frac{L}{4}[\Delta\phi(N + \Delta N) + \Delta N(\phi + \phi_0)] \tag{33}$$

(e) Given the two computed values of Δe a new value of $\Delta\phi$ is chosen according to the secant rule and the analysis goes back to step (b), unless the equilibrium error lies within a prescribed tolerance.

The model validation has been obtained through a series of experimental tests; the test results and comparison with numerical simulations are described in detail in References 4 and 6.

4. ANALYSIS OF DYNAMIC RESPONSE TO SEISMIC EXCITATION

In the case of single-component seismic excitation, the equations of motion of an N degree-of-freedom system showing material non-linearities can be written in the matrix form

$$[m]\{\ddot{v}\} + [c]\{\dot{v}\} = \{R\} - [m]\{r\}a(t) \tag{34}$$

where $[m]$ and $[c]$ are, respectively, the inertia and damping matrices $\{v\}$ is the configuration vector, $\{R\}$ is the vector of generalized components of internal restoring forces, $\{r\}$ is a vector having unit coefficients along those co-ordinates which act in the same direction as the excitation and zero coefficients elsewhere and $a(t)$ is the ground acceleration. The generalized components of the restoring forces are, in general, of the type

$$\{R\} = \{R(v_1, \ldots, v_N, \dot{v}_1, \ldots, \dot{v}_N, z_1, \ldots, z_M)\}$$

the z_j's being the relevant internal variables for the adopted non-linear models.

The solution of the non-linear equations of motion have been carried out by means of the step-by-step technique described in Reference 11; this is an implicit procedure whose main features can be summarized as follows.

(1) Integration is performed by means of the classical Newmark method (see Reference 12 for an excellent review on the topic) as modified by Hilber *et al.*[13] to include numerical dissipation of high frequency response.

(2) At the end of the Newmark time-step (time t_{n+1}) the following equilibrium check is performed

$$\|\{e\}_{n+1}\| \leqslant \varepsilon_1 \|[m]\{r\} a_{n+1}\| \tag{35}$$

where $\|\{e\}_{n+1}\|$ is the euclidean norm of the equilibrium error vector, a_{n+1} is the ground acceleration at time t_{n+1} and ε_1 is a prescribed tolerance.

(3) If the condition (35) is not satisfied the classical 'modified Newton–Raphson' (MNR) iterative scheme is adopted to ensure equilibrium; this is based upon the recursive evaluation of configuration corrections, obtained, at iteration k, as the solution of the linear equations:

$$[\hat{k}^t]_n \{\Delta v\}_{n+1}^{(k+1)} = \{e\}_{n+1}^{(k)} \tag{36}$$

where $[\hat{k}^t]_n$ is the tangent stiffness matrix at the end of the previous step (time t_n), $\{\Delta v\}_{n+1}^{(k+1)}$ is the configuration correction and $\{e\}_{n+1}^{(k)}$ is the equilibrium error after iteration k.

(4) To check convergency during the MNR iteration process an energy-based convergency criterion is applied; at the first iteration a reference energy value W_0 is computed as

$$W_0 = \{e\}_{n+1}^{(0)^T} \{\Delta v\}_{n+1}^{(1)} \tag{37}$$

while at subsequent iterations convergency is checked against tolerance ε_2 by means of the inequality

$$W_k = \{e\}_{n+1}^{(k-1)^T} \{\Delta v\}_{n+1}^{(k)} \leqslant \varepsilon_2 W_0 \tag{38}$$

(5) Consistently with the MNR iteration scheme, the so-called 'path-independent state determination' criterion[14] is adopted in the computation of the restoring forces $\{R\}_{n+1}^{(k)}$ during the iteration; according to the criterion, restoring force increments are obtained as functions of the sum of the displacement corrections computed during the previous iterations, and not summing up force increments. Analytically, this results in the adoption of the formulas

$$\{R\}_{n+1}^{(k)} = \{R\}_n + \{\Delta R\}_{n+1}^{(k)} \tag{39}$$

$$\{\Delta R\}_{n+1}^{(k)} = \{\Delta R(\{\Delta v\}_{n+1}^{(k,\text{tot})})\}_{\{v\}_n, \{\dot{v}\}_n, \{z\}_n} \tag{40}$$

$$\{\Delta v\}_{n+1}^{(k,\text{tot})} = \sum_{s=0}^{k} \{\Delta v\}_{n+1}^{(s)} \tag{41}$$

For the cases of slow convergency[15] and to face problems related to the hysteretic behaviour of the adopted elements (e.g. more than two events in one time step for a single beam element) the possibility has been also implemented to subdivide the time interval into smaller integration steps.

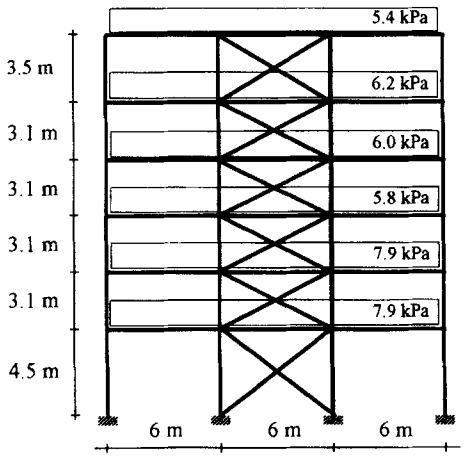

Figure 7. Example of three-bay plane frame: overall dimensions and design loads

5. EXAMPLES OF APPLICATION

5.1. Design of the CS1 combined system

The CS1 system is depicted in Figure 7; it consists of a three-bay frame in which only the central bay is designed as an MRF. As it concerns ultimate limit states (ULS) the MRF has been sized by neglecting the contribution of the diagonal bars, on the basis of the following input data:

(1) frame to frame spacing of five meters;
(2) top four stories intended for residential use (live load 1·4–1·8 kN/m^2);
(3) roof live load (snow) 1 kN/m^2;
(4) bottom two stories for office use (live load 3·5 kN/m^2);
(5) design seismic action as specified by EC8[1] for a soil profile type B, a peak ground acceleration (PGA) $a_0 = 0{\cdot}35$ g, a damping ratio of 3 per cent and a behaviour factor $q = 6$.

Given the above input data, the MRF design was carried out by performing the steps summarized as follows.

Step 1: Preliminary member sizing was based upon the simplified analysis method proposed in EC8;[1] according to this procedure equivalent static forces are applied which are linearly distributed along the structure height and whose sum equals the total base shear computed via the design spectrum and a first natural period estimate.

Step 2: The system of equivalent lateral forces was subsequently used to check the frame collapse mechanism. The load multipliers pertaining to the partial mechanisms of Figure 8 were computed for each storey, and members' sizes were modified in order to make these values larger than the multiplier corresponding to the activation of the desired complete sidesway mechanism. The latter multiplier was computed by taking second-order effects into account.

Step 3: Concentrical braces were introduced in the design and the combined system was checked, via response spectrum analysis, against the following requirements.

(a) Serviceability limit state (SLS) requirements as specified by EC8[1] as

$$d_r \leqslant \delta h v; \qquad d_r = q_d d_e \gamma_1 \tag{42}$$

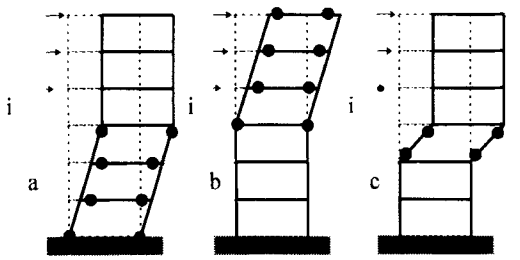

Figure 8. Storey collapse mechanisms for a moment-resisting frame

where d_r is the interstory drift, h the storey height, ν the coefficient taking account of the lower return period of the event associated to the SLS, d_e is the interstory drift computed via the ULS design spectrum, q_d is the displacement behaviour factor, γ_I the importance factor and where the following values were assumed

$$\delta = 0{\cdot}004,\ 0{\cdot}006; \qquad \nu = 2, \qquad q_d = q = 6, \qquad \gamma_I = 1 \tag{43}$$

(b) Ductility requirements for the braces, which were stated as a limit ductility demand of 1·5 under the SLS event.
(c) Resistance and stability of columns against the axial forces transmitted by the diagonal bars.

Note that in computing the response of the combined system the contribution of the compressed brace has been taken into account, as proposed in Reference 6, by multiplying its area by the coefficient of reduction of the compressive load capacity χ as stated by curve 'c' in Eurocode 3.[16] To maintain symmetry, the area of the two diagonal bars at each interstory has been defined, in the dynamic model used for response spectrum analysis, according to the following formula

$$\bar{A}_d = \frac{A_d(1 + \chi)}{2} \tag{44}$$

where A_d is the gross section of the bars. The design axial force in each column was subsequently computed, on the basis of the values $\bar{N}_c$ (column axial force) and $\bar{N}_d$ (diagonal axial force) resulting from the response of the symmetric model, according to the relation

$$N_c = \bar{N}_c + \frac{1 - \chi}{1 + \chi}\bar{N}_d \tag{45}$$

As a result of the design process for the most severe condition $\delta = 0{\cdot}004$ [see equations (42), (43)], columns at the first storey were such that the condition in Step 2 could not be completely met and the final collapse mechanism for the MRF structure was of the type of Figure 8(b) at the first floor (incomplete sidesway mechanism with 'strong' first storey). The same column design was maintained subsequently for the more favourable case $\delta = 0{\cdot}06$, while diagonal braces were obviously different. Table I contains the floor masses and member sections for the CS1 system.

Finally, the PGA corresponding to the attainment of the resistance of the most stressed element has been evaluated from the elastic spectrum [EC8-curve 'b'] and from the vertical loads. The value found was equal to 0·5985 m s^{-2}; given the linear law relating, for a given structure, the design PGA and the behaviour factor, in Table II, for the CS1 system with no braces, the values of PGA are shown correspoding to different values of the q-factor. The PGA value for $q = 6$ is slightly higher than the design value $a_0 = 0{\cdot}35$ g due to unavoidable oversizing of structural elements. The PGA values of Table II were used in the dynamic analysis of the structure to normalize, at different levels of ductility demand, the accelerograms used as seismic input representing the ULS event.

Table I. CS1 system. Floor masses and member sections

f. l.	(Masses) (kg)	Columns	Beams	Braces	
				$\delta = 0{\cdot}004$	$\delta = 0{\cdot}006$
1	44325	HE 340 M	HE 280 B	2 UPN 80	2 UPN 40
2	44325	HE 340 B	HE 280 B	2 UPN 100	2 UPN 65
3	42300	HE 300 B	HE 260 B	2 UPN 100	2 UPN 50
4	42300	HE 300 B	HE 240 B	2 UPN 100	2 UPN 40
5	45000	HE 280 B	HE 240 B	2 UPN 80	2 UPN 30
6	42300	HE 260 B	HE 220 B	2 UPN 65	2 UPN 30

Table II. CS1 system. Design PGA vs. design q-factor

q	a_0 (m/s^2)
1	0·5985
4	2·3941
5	2·9927
6	3·5912
7	4·1898
8	4·7883

5.2. Numerical analysis of the seismic behaviour of the CS1 combined system

The dynamic model used in the numerical analysis of the seismic behaviour of the CS1 system is depicted in Figure 9. The model mass matrix was obtained, under the hypothesis of rigid diaphragm floor behaviour, assuming that inertia is concentrated at the storey levels; the viscous damping matrix was computed, according to the proportionality assumption, imposing a value of 0·03 to the damping factors of all the elastic normal modes.

The beam model described in Section 2 was used to model flexural beams; the yielding moment of the section was taken as equal to the fully plastic moment, while the other coefficients describing the hysteretic law of the plastic hinges (PHs) were taken from experimental results regarding elements of the same series having similar width-to-thickness ratios.

The same element was employed for column modelling too; this introduces two kinds of approximations. First of all, axial-load–bending-moment interaction was neglected and the full plastic moments of the column sections was computed on the basis of static axial loads; this approximation, which is usually accepted for MRFs due to symmetry properties, can be regarded as reasonable for a braced frame, as the CS1, where diagonal members are relatively weak and columns are remarkably strong due to capacity design considerations. Secondly, the other coefficients controlling the columns' PH hysteretic behaviour were taken from experimental tests performed with zero axial loads; this assumption was accepted since the largest part of energy dissipation occurs in beams and braces. Moreover, the unavoidable inelastic cycling in columns is characterized by excursions which are limited in amplitude and number.

The non-linear truss element described in Section 3 was employed for the braces; each of them is modelled by means of a single element, while the midspan connection is taken into account by assuming an unsupported length half the actual diagonal bar length. A 'death' option was also implemented in the non-linear truss element such that, whenever a brace reaches in tension a specified ultimate ductility demand, it is removed from the dynamic model for the subsequent part of the analysis; ultimate ductility values $\mu_{d,u}$ equal to 2, 4, 6, 8 and infinity were considered.

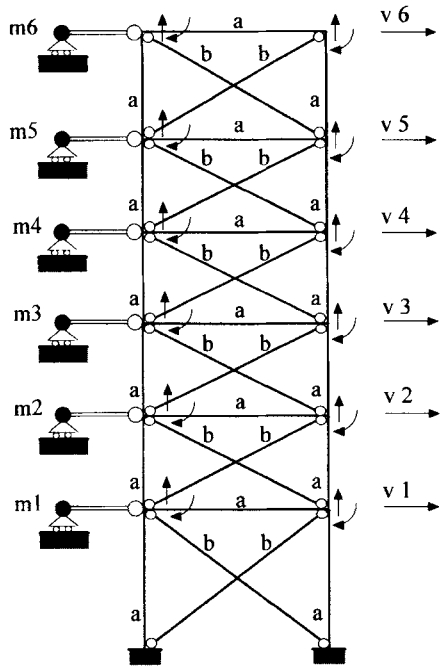

Figure 9. Dynamic model of the CS1 system, where a = non-linear beam and b = non-linear brace

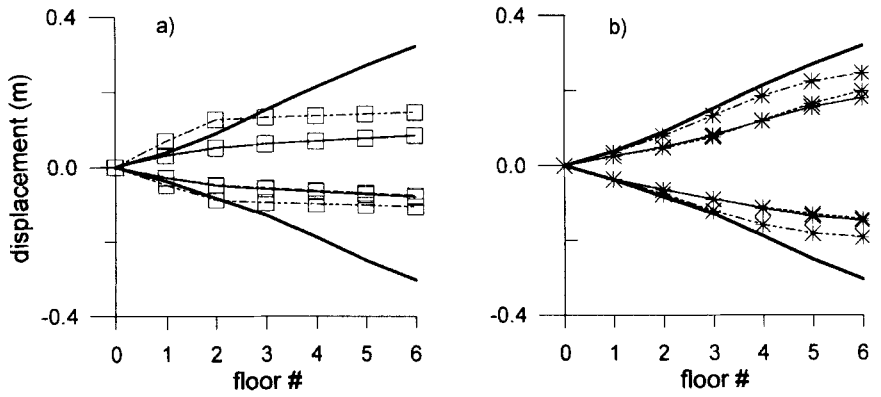

Figure 10. CS1 system. Floor displacement envelope for $q = 6$. (a) $\delta = 0{\cdot}004$; (b) $\delta = 0{\cdot}006$. ——— MRF only; ——— $\mu_{d,u} = \infty$; – – – – $\mu_{d,u} = 8$; – – – $\mu_{d,u} = 6$; – – – – – $\mu_{d,u} = 4$; – – – – – – $\mu_{d,u} = 2$

The above described dynamic model was subjected to horizontal base acceleration; five different artificial accelerograms which are compatible with the EC8-curve 'b' elastic spectrum were considered. These time-histories, which were generated according to the technique described in Reference 6, are consistent with the hypothesis that the ground acceleration is an uniformly modulated non-stationary process. The input motion was scaled, for each value of the design q-factor, to the PGA values listed in Table II. Unless otherwise specified, all values of response parameters shown in the following have been computed as mean extreme values over the five seismic input realizations.

In Figure 10 the envelopes of maximum values of floor displacements are shown, for the case $q = 6$, for the two values $\delta = 0{\cdot}004$ and $\delta = 0{\cdot}006$ of the interstory drift factor and for all cases of diagonal ultimate

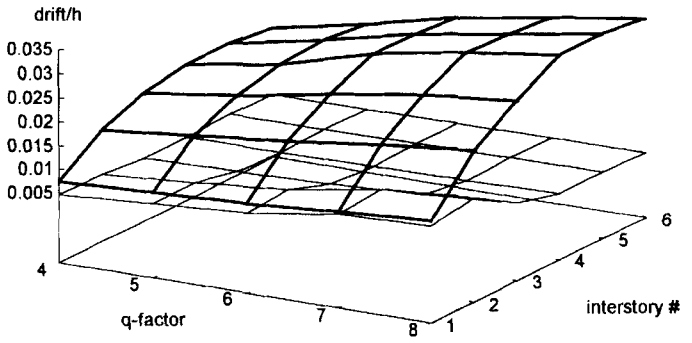

Figure 11. CS1 system $\delta = 0{\cdot}004$. Non-dimensional interstory drift vs. q-factor. ——— MRF only; ——— $\mu_{d,u} = 4$

ductility $\mu_{d,u}$; curves corresponding to the bare MRF are depicted for comparison. Examination of the other curves suggests the following considerations.

(i) The displacement envelope for the case $\delta = 0{\cdot}004$ and $\mu_{d,u} = 2$ shows impressive relative drifts, more than 50 per cent larger than those of the unbraced MRF, at the lower two interstories. The phenomenon did not occur in the case of $\delta = 0{\cdot}006$ where, however, the envelope corresponding to $\mu_{d,u} = 2$ is remarkably less favourable than those of the other braced frames.

(ii) The curves describing the behaviour of braced frames for $4 \leqslant \mu_{d,u} \leqslant 8$ are practically identical in Figure 10(a) and very similar in 10(b), showing little influence of the ultimate diagonal ductility in this range of values.

(iii) The diagonal bracing, though introduced for adequacy of SLS prescriptions, is very effective, except for the case $\mu_{d,u} = 2$, in reducing floor displacement for the ULS event as well.

(iv) The displacement reduction is obviously more marked for 'the system designed against the value $\delta = 0{\cdot}004$; if we look at the first floor displacement, however, we observe a less significant reduction also for cases with $4 \leqslant \mu_{d,u} \leqslant 8$, this showing a tendency to concentrate inelastic response in the lower storey.

Based upon the first of the above considerations it has been decided to discard, in the following presentation of the results, the system in which diagonals have ultimate ductility equal to two, since its behaviour does not seem to posses adequate reliability. By the design standpoint, this means mainly that the diagonal end connections must posses adequate overstrength and ductility; note that this provision is not as severe as in normal CBF systems since here, with no slenderness limitations, the resistance of diagonal bars is limited.

In the 3-D plots of subsequent Figures 11 and 12, non-dimensional interstory drifts (drift-to-height ratios) are shown against design q-factors; comparison is made between the bare MRF case and the braced case with $\mu_{d,u} = 4$. It can be again noted how, for the case $\delta = 0{\cdot}004$ (Figure 11) the non-dimensional relative drift is mostly concentrated at the first and second interstories, where it increases with the q-factor reaching values of about 0·012–0·013 for $q = 8$; in the upper portion of the frames, drifts are very moderate and remain practically constant with respect to the design q-factor.

The behaviour of the system designed for $\delta = 0{\cdot}006$ (Figure 12) is very different, since relative drift tends to be higher in upper stories, where it almost reaches the values of the unbraced MRF (order of 0·03); globally, the lateral displacement appears much better distributed along height than in Figure 11 and shows a more marked and regular tendency to increase with the q-factor value.

In Figure 13, the overall maximum column plastic hinge (PH) rotation, defined as the extreme value which has occurred in any of the vertical bars for any of the artificial accelerograms, is plotted against the q-factor; for the more weakly braced system ($\delta = 0{\cdot}006$) rotations exceed those of the unbraced frames. It can be observed, however, that the two curves run remarkably parallel and for $q = 6$ the rotation does not exceed

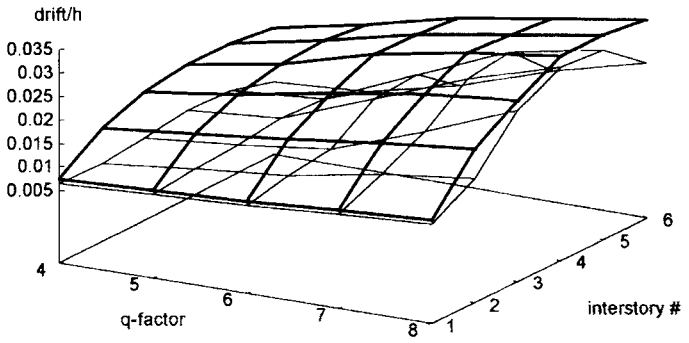

Figure 12. CS1 system $\delta = 0{\cdot}006$. Non-dimensional interstory drift vs. q-factor. ———— MRF only; ——— $\mu_{d,u} = 4$

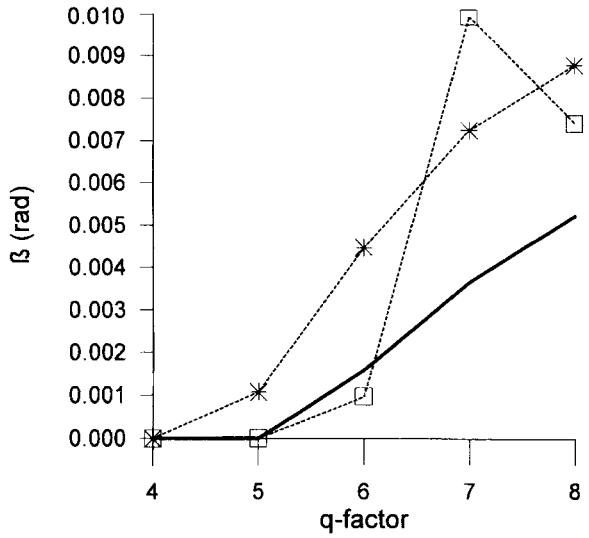

Figure 13. CS1 system. Maximum overall plastic rotation in columns vs. q-factor. (□) $\delta = 0{\cdot}004$; (*) $\delta = 0{\cdot}006$. ———— MRF only; ----- $\mu_{d,u} = 4$

the value of 0·005 rad. The behaviour of the other frame ($\delta = 0{\cdot}004$) is different; up to the design value $q = 6$ rotations are smaller than those of the unbraced MRF, while for higher values of the behaviour factor the tendency to develop a soft-storey causes a sharp increase in the plastic deformations, which exceed , for $q = 7$, also those of the weaker system.

Subsequent Figures 14 and 15 are devoted to beams behaviour; in the first one the overall maximum PH rotations (same meaning as above) are plotted for all considered values ($\mu_{d,u}$ equal to 4, 6 and 8) of ultimate diagonal ductility in the case $q = 6$. For the latter level of excitation it can be seen that in the braced system designed for $\delta = 0{\cdot}004$ there are virtually no plastic rotations in beams, except very low values (around 0·002–0·003 rad) at the lower two stories. In the other case ($\delta = 0{\cdot}006$) PH rotations are larger, especially in the case $\mu_{d,u} = 4$, but always smaller than those of the unbraced frame. Note that there is no graphical difference among results obtained for ultimate ductility $\mu_{d,u}$ ranging from six to infinity.

To help the reader in the quantitative appreciation of the results of Figure 14, and of the following ones, it can be reminded that the value of 0·015 rad is usually assumed (see Reference 3) as a minimum value of plastic rotation capability in order to justify behaviour factors of the order of six; we note that this value is exceeded, for $q = 6$, only by the MRF without braces.

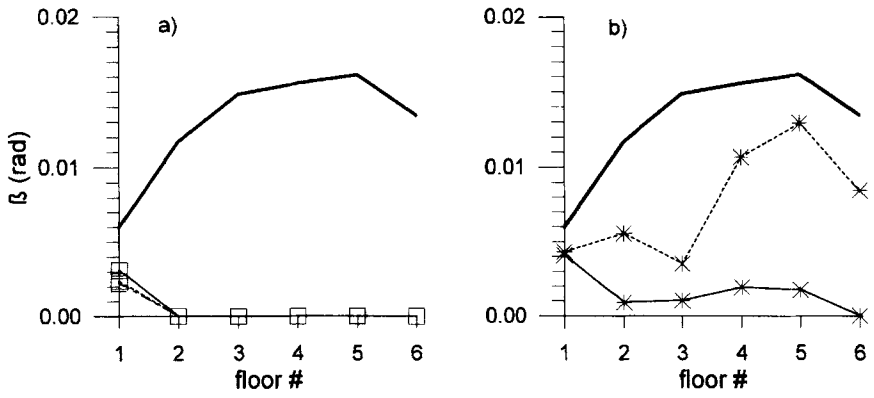

Figure 14. CS1 system. Maximum overall plastic rotation in beams vs. floor for q-factor $=6$. (a) $\delta = 0{\cdot}004$; (b) $\delta = 0{\cdot}006$. ——— MRF only; ——— $\mu_{d,u} = \infty$; - - - - - - $\mu_{d,u} = 8$; — — — $\mu_{d,u} = 6$; · · · · $\mu_{d,u} = 4$

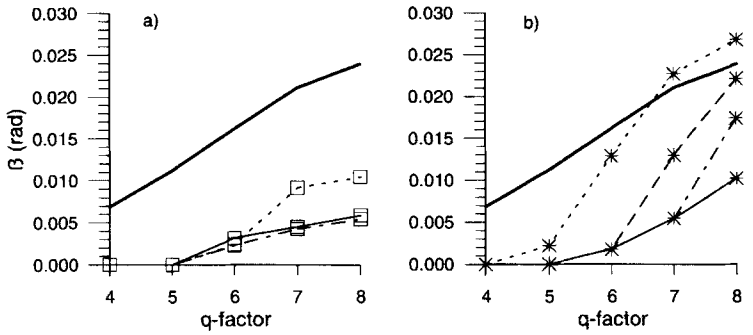

Figure 15. CS1 system. Maximum overall plastic rotation in beams vs. q-factor. (a) $\delta = 0{\cdot}004$; (b) $\delta = 0{\cdot}006$. ——— MRF only; ——— $\mu_{d,u} = \infty$; - - - - - $\mu_{d,u} = 8$; — — — $\mu_{d,u} = 6$; - - - - - - $\mu_{d,u} = 4$

The subsequent Figure 15 shows the overall maximum value of PH rotation against the q-factor value. From Figure 15(a) ($\delta = 0{\cdot}004$) it can be noted that, for $q \leqslant 8$, the maximum PH rotations are all below the value 0·010 rad.

For the system designed for $\delta = 0{\cdot}006$ [Figure 15(b)] PH rotations are much higher and the reference value of 0·015 rad is exceeded, for $q \geqslant 6$, by all systems except the one having braces of infinite ductility; again, all braced frames show, for $q < 7$, PH rotations which are smaller than those of the MRF.

In judging the behaviour of the CS1 system it must be noted that the seismic loading condition to which the braced MRF is subjected is very severe because of the fact that lateral bays of the frame do not resist lateral forces; some recent tests regarding a complete two-bay MRF with diagonal bars bracing one of the bays, designed with the same criteria as the CS1 system, have shown a more favourable structural behaviour, with respect to both the ULS and SLS design events.

In Figures 16 and 17, finally, examples are given of the non-linear behaviour of the dissipative elements; in the first the moment–rotation hysteretic behaviour of the base column PH for $q = 6$ and $\delta = 0{\cdot}004$ is shown. For the same case in Figure 17 the axial force in one of the braces at the first floor is plotted against the non-dimensional (i.e. divided by the bar length) relative end displacement.

5.3. Design of the CS2 combined system

The CS2 system is characterized by the same design input data and overall dimensions as the CS1 frame; the central bay, however, is now designed as a CBF, on the basis of a behaviour coefficient $q = 4$. The

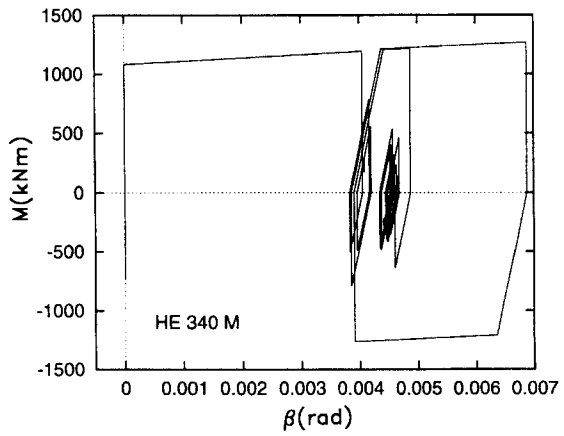

Figure 16. CS1 system. Example of column plastic hinge hysteretic behaviour for $q = 6$

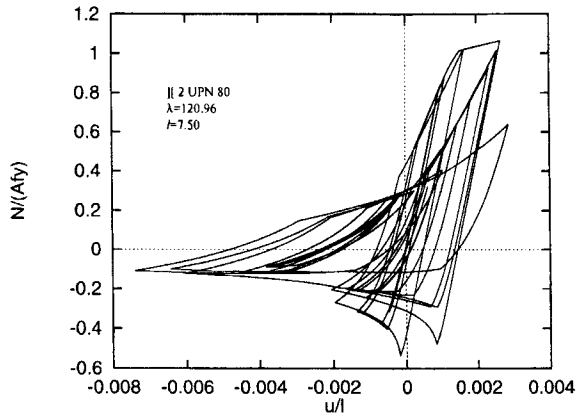

Figure 17. CS1 system. Example of brace hysteretic behaviour for $q = 6$

Table III. CS2 system. Overstrength factors $A_d(1 + \chi)f_y/N_d$ in diagonal braces design. $a_0 = 0{\cdot}35$ g; $q = 4$

	$\delta = 0{\cdot}004$		$\delta = 0{\cdot}006$	
f. 1.	Initial	Modified	Initial	Modified
1	1·44	1·70	1·26	1·23
2	2·03	2·03	1·22	1·20
3	2·30	2·29	1·37	1·35
4	2·76	2·68	1·33	1·33
5	3·15	3·11	1·45	1·45
6	3·02	2·96	2·56	2·65

member sizing has been carried on following the EC8 specifications. Two values (0·04 and 0·06) of the interstory drift coefficient δ were assumed, thus leading to two different CBF designs.

Since in previous research works (see for example Reference 6) 'soft-storey' behaviour appeared to be critical, the problem of structural regularity was given particular attention: to this purpose in Table III the

Table IV. CS2 system. Member sections

		$\delta = 0{\cdot}004$				$\delta = 0{\cdot}006$			
		Initial		Modified		Initial		Modified	
f. 1.	Beams	Columns	Braces	Columns	Braces	Columns	Braces	Columns	Braces
1	HE 140 B	HE 450 B	2 UPN 140	HE 450 B	2 UPN 160	HE 450 B	2 UPN 120	HE 450 B	2 UPN 120
2	HE 140 B	HE 300 B	2 UPN 160	HE 320 B	2 UPN 160	HE 300 B	2 UPN 100	HE 320 B	2 UPN 100
3	HE 140 B	HE 260 B	2 UPN 160	HE 280 B	2 UPN 160	HE 260 B	2 UPN 100	HE 280 B	2 UPN 100
4	HE 140 B	HE 220 B	2 UPN 160	HE 260 B	2 UPN 160	HE 220 B	2 UPN 80	HE 260 B	2 UPN 80
5	HE 140 B	HE 180 B	2 UPN 140	HE 220 B	2 UPN 140	HE 180 B	2 UPN 65	HE 220 B	2 UPN 65
6	HE 140 B	HE 140 B	2 UPN 80	HE 220 B	2 UPN 80	HE 140 B	2 UPN 65	HE 220 B	2 UPN 65

Table V. CS2 system. Design PGA vs. design q-factor

CS2 q	$\delta = 0{\cdot}004$ a_0 (m/s^2)	$\delta = 0{\cdot}006$ a_0 (m/s^2)
1	1·4324	1·04293
2	2·8644	2·0858
3	4·2974	3·1288
4	5·7298	4·1717
5	7·1623	5·2146
6	8·5948	6·2576

overstrength ratios are listed, defined as the ratio of the 'best-estimate' bracing system resistance (computed according to the effective area (44)) to the design interstory shear. For each value of δ the first column contains the values obtained according to the EC8 design procedure, while the second column lists the values obtained after modifying the member sizing to achieve better regularity properties. The results of this process are summarized in Table IV, where the element section types are listed for the initial and final sizing. Note that, in spite of the modification, the system designed for $\delta = 0{\cdot}006$ shows higher regularity; this difference was left purposefully to investigate the influence of the regularity properties.

Finally, the PGA corresponding to the attainment of the design resistance in the most stressed interstory was evaluated; with the same criteria as for the CS1 system, in Table V the values of PGA are shown corresponding, for the two values of δ, to different values of the q-factor. It can be noted that for the value $q = 4$ of the design behaviour factor, the 'actual' PGA is much higher than the design value ($a_0 = 0{\cdot}35$ g); this is due to the severity of the SLS deformability requirements, which govern member sizing, leading to considerable overstrength in the structural elements. This means that, by converse, the 'actual' value of the q-factor associated to a given design PGA is much lower than the design value. Note that this did not happen for the CS1 system where the 'seismic resistant' structure (that is the MRF) was not affected by the SLS requirements.

5.4. Numerical analysis of the seismic behaviour of the CS2 combined system

The seismic behaviour of the CS2 systems was simulated by means of the dynamic model shown in Figure 18. The model is formulated according to the same criteria as mentioned for the CS1 systems; beams are here regarded as hinge-ended elements. Columns are modelled by means of one-component elements, assuming that maximum flexural stiffness lies in the frame plane; to test the influence of the column continuity and resistance, four cases have been studied. In the first (case 0), columns have pinned connections at each floor; in the other cases, columns are continuous. Their flexural resistance is computed, given the static axial force N_{st}, for the values N_{st} (case 1), $2N_{st}$ (case 2) and $3N_{st}$ (case 3). Note that the latter value is close to the maximum total (static plus dynamic) axial force that was subsequently obtained from the dynamic simulations.

Dynamic analyses were carried out under the same criteria as described for the CS1 systems; the simulated accelerograms were scaled, for each design q-factor considered, to the values of PGA listed in Table V.

In Figure 19 the floor displacement envelopes are shown, in the case $q = 4$ (actual value), for the two structures designed for the values $\delta = 0{\cdot}004$ and $\delta = 0{\cdot}006$ of the interstory drift factor and for the above quoted cases 0, 1, 2 and 3. As it can be easily noted the behaviour of the two structures is very different; the bracing system designed for $\delta = 0{\cdot}004$, though more resistant, shows a typical soft-storey behaviour, while for the other structure ($\delta = 0{\cdot}006$) dynamic response showed much better regularity in elevation. As it concerns column flexural resistance, the influence on extremes of displacements appears very small in both cases.

The same considerations can be drawn for Figure 20, where the top displacement is plotted against the actual q-factor; though the extreme top displacement is very similar, the case $\delta = 0{\cdot}004$ shows a much larger first floor displacement and a smaller effect of column resistance modelling.

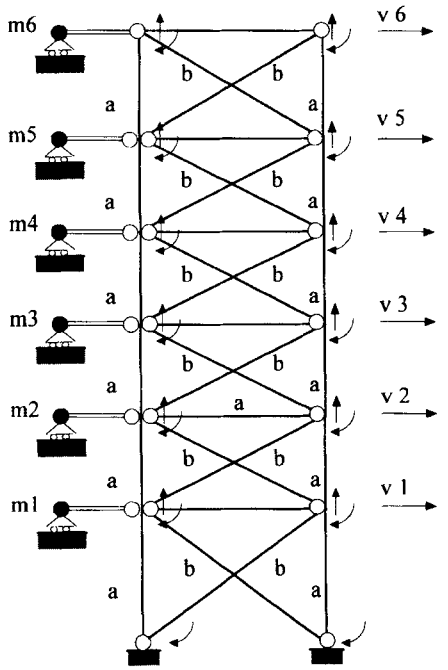

Figure 18. Dynamic model of the CS2 system, where a = non-linear beam and b = non-linear brace

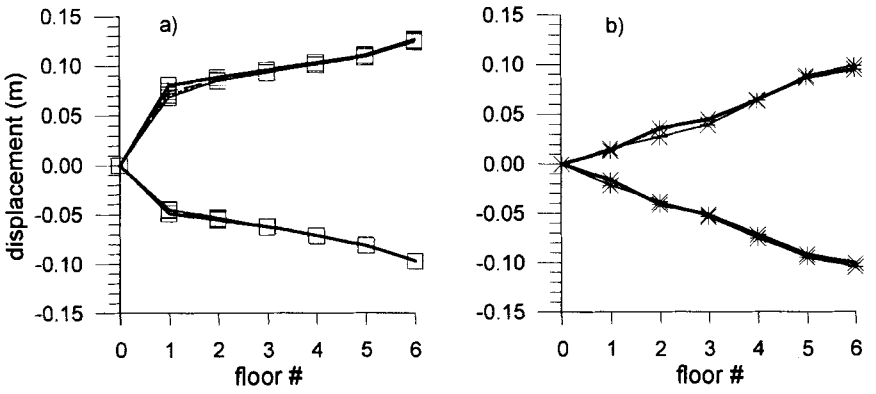

Figure 19. CS2 system. Floor displacement envelope for $q = 4$. (a) $\delta = 0{\cdot}004$; (b) $\delta = 0{\cdot}006$. ——— case 0; ——— case 1; - - - - case 2; ------ case 3

The above phenomena can be more easily appreciated from the 3-D plots of Figures 21 and 22 where the maximum ductility demand in diagonal braces of cases 0 and 3 is shown, for each interstory, against the actual q-factor. The behaviour of the two systems is almost opposite; for the case $\delta = 0{\cdot}004$ (Figure 21), and for both column models, ductility demand is concentrated at the first interstory, where values of 10–12 are reached, and at the last one, with lower values from two to four. The remaining part of the structure remains essentially elastic. In the case $\delta = 0{\cdot}006$ (Figure 22) the system seems to succeed in exploiting the column flexural resistance; in case 3, in fact, the ductility demand is more 'smeared' over the structure and the peaks at the second and fifth interstories are greatly attenuated at the highest q-factor values. In all cases, ductility peaks are lower than those of Figure 21. Note that the hypothesis adopted in case 3 for column resistance is very severe (yield moment computed for $N = 3N_{st}$); the response, however, is very similar in cases 1 and 2.

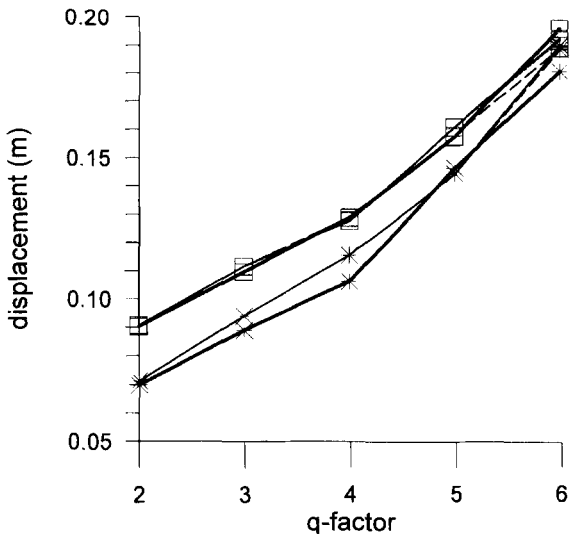

Figure 20. CS2 system. Top floor displacement vs. q-factor. (□) $\delta = 0{\cdot}004$; (*) $\delta = 0{\cdot}006$. ——— case 0; ····· case 1; - - - - case 2; ------ case 3

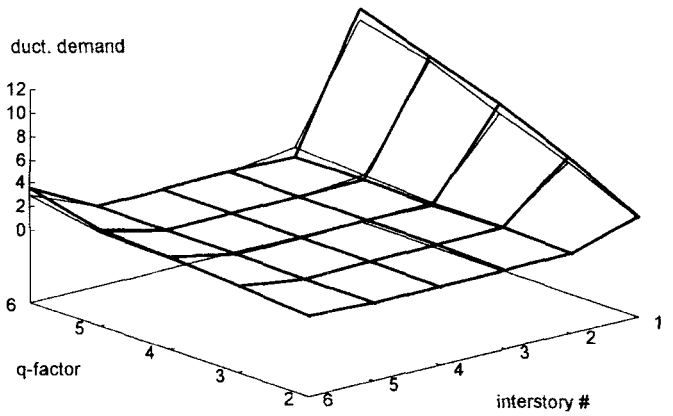

Figure 21. CS2 system. Braces ductility demand vs. q-factor. $\delta = 0{\cdot}004$. ——— case 0; ——— case 3

Finally, in Figure 23 the maximum plastic rotations in columns are plotted, for the two systems and for case 3, against the actual q-factor; note that in the case $\delta = 0{\cdot}006$ there are four interstories with columns undergoing plastic rotations with small maximum values (less than 0·001 rad for $q < 4$ and less than 0·005 rad for $q < 6$). In the case $\delta = 0{\cdot}004$ the maximum plastic rotations, all occurring at the first interstory, show large values (greater than 0·01 rad) for q larger than 3·5.

6. CONCLUSIONS

In the research work described here the non-linear seismic behaviour of steel frames has been analysed, by addressing several issues pertaining to both structural analysis and design.

From the analysis point of view, a non-linear beam element has been developed based upon a classical lumped plasticity approach; the hysteretic relation of the inelastic hinges at the ends of the element has been

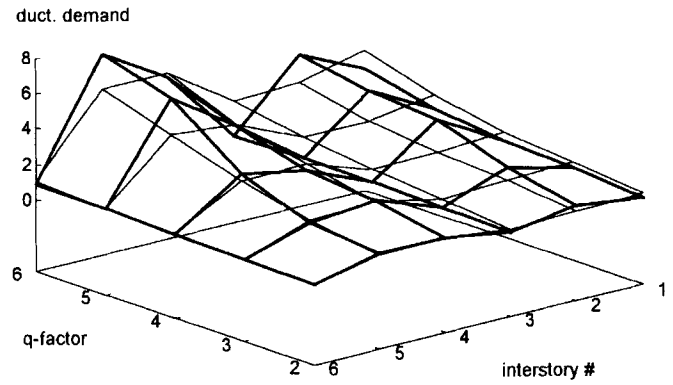

Figure 22. CS2 system. Braces ductility demand vs. q-factor. $\delta = 0{\cdot}006$. ——— case 0; ——— case 3

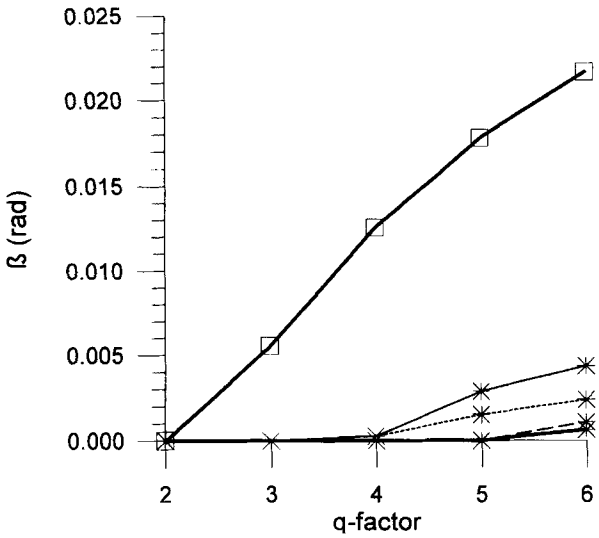

Figure 23. CS2 system. Maximum overall plastic rotation in columns vs. q-factor for case 3. (□) $\delta = 0{\cdot}004$; (*) $\delta = 0{\cdot}006$. ——— 2nd storey; ——— 3rd storey; ----- 4th storey; ---- 5th storey

determined on the basis of experimental tests on cantilever members. This relation accounts for isotropic hardening, for strength degradation due to local buckling and low-cycle fatigue and for stiffness degradation due to damage accumulation. In the paper, the technique adopted for deriving the moment–rotation hysteretic law of the flexural hinge starting from the experimental results has been described; the solution of the problems related to the implementation of the element within a step-by-step implicit integration procedure has been presented.

Coming to the design issues, MRF systems have been first considered by focusing attention on the problem of serviceability requirements under moderate earthquakes. An MRF has been designed according to Eurocode 8, without checking serviceability (interstory drifts) provisions against moderate earthquakes; these have been subsequently satisfied by adding diagonal braces which are not considered in the ultimate conditions. Note that the latter elements do not satisfy EC8 requirements for bracing members (e.g. for slenderness). The non-linear behaviour of the combined system under ultimate seismic conditions have been favourably compared, by repeated numerical simulations, to that of the unbraced MRF, under the condition that diagonals possess an ultimate ductility equal, at least, to four.

Finally, the behaviour of CBFs has been considered to investigate the effect of the column flexural resistance, which is usually disregarded in the design, on the response to extreme events. The results show the utmost importance of structural regularity; lack of this property causes 'soft-storey' behaviour such as to overshadow any other response effect. When strict regularity conditions are met, on the contrary, the effect of the flexural resistance of columns allows for a more favourable distribution of ductility demand throughout the bracing system.

ACKNOWLEDGEMENTS

The authors gratefully thank Professor Giulio Ballio of the Department of Structural Engineering of Politecnico di Milano for his fundamental suggestions about the design aspects of the research. The financial contribution from the Italian Ministry of University and Scientific and Technological Research (MURST) is also acknowledged.

REFERENCES

1. 'Eurocode no. 8: Common unified rules for structures in seismic regions', *ENV 1998-1-1*, 1994.
2. 'Recommended lateral force requirements and commentaries', Seismology Committee, Struct. Eng. Assoc. of California, Sacramento, California, 1990.
3. V. V. Bertero, J. C. Anderson and H. Krawinkler, 'Performance of steel building structures during the Northridge earthquake', *Report No. UCB/EERC-94/09*, EERC, University of Calilfornia at Berkeley, 1994.
4. G. Ballio and F. Perotti, 'Cyclic behaviour of axially loaded members: numerical simulation and experimental verification', *J. construct. steel res.* **7**, 3–41 (1987).
5. A. Astaneh-Asl and S. C. Goel, 'Cyclic in-plane buckling of double angle bracing', *ASCE, j. struct. eng.* **110**, 2036–2055 (1984).
6. F. Perotti and G. P. Scarlassara, 'Concentrically braced steel frames under seismic actions: non-linear behaviour and design coefficients', *Earthquake eng. struct. dyn.* **20**, 409–427 (1991).
7. G. Ballio and C. A. Castiglioni, 'Seismic behaviour of steel sections', *J. construct. steel res.* **29**, 21–54 (1994).
8. M. F. Giberson, 'Two nonlinear beams with definition of ductility', *ASCE, j. struct. div.* **95**, 137–157 (1969).
9. C. A. Castiglioni, N. Di Palma and E. Moretta, 'A trilinear constitutive model for the seismic analysis of steel structures', *Costruzioni Metalliche* No. 2, 80–96 (1990).
10. C. A. Castiglioni and N. Di Palma, 'Steel members under cyclic loads: numerical modelling and experimental verifications', *Costruzioni Metalliche* No. 6, 3–27 (1988).
11. F. Perotti, A. De Amici and P. Venturini, 'Numerical analysis and design implications of the seismic behaviour of one-storey steel bracing systems', *Eng. struct.* **18**, 162–178 (1996).
12. J. Agryris and H.-P. Mlejnek, *Dynamics of Structures*, North-Holland, Amsterdam, 1991.
13. H. M. Hilber, T. J. R. Hughes and R. L. Taylor, 'Improved numerical dissipation for time integration algorithms in structural dynamics', *Earthquake eng. struct. dyn.* **5**, 283–292 (1977).
14. D. P. Mondkar and G. H. Powell, 'ANSR-I general purpose program for analysis of nonlinear structural response', *Report No. UCB/EERC-75/37*, EERC, University of California at Berkeley, 1975.
15. M. Geradin, M. Hogge and S. Idelsohn, 'Implicit finite element methods', in T. Belytschko and T. J. R. Hughes (eds), *Computational Methods for Transient Analysis*, Elsevier, Amsterdam, 1983.
16. 'Eurocode No. 3: Common unified rules for steel structures', *ENV 1993-1-1*, 1993.